

Specular neutron reflectivity and the structure of artificial protein maquettes vectorially oriented at interfaces

Joseph Strzalka,¹ Brian R. Gibney,² Sushil Satija,³ and J. Kent Blasie¹¹*Department of Chemistry, University of Pennsylvania, Philadelphia, Pennsylvania 19104-6323, USA*²*Department of Chemistry, Columbia University, New York, New York 10027, USA*³*NIST Center for Neutron Research, Gaithersburg, Maryland 20899, USA*

(Received 3 May 2004; published 9 December 2004)

Artificial peptides can be designed to possess a variety of functionalities. If these peptides can be ordered in an ensemble, the functionality can impart macroscopic material properties to the ensemble. Neutron reflectivity is shown to be an effective probe of the intramolecular structures of such peptides vectorially oriented at an interface, key to ensuring that the designed molecular structures translate into the desired material properties of the interface. A model-independent method is utilized to analyze the neutron reflectivity from an alkylated, di- α -helical peptide, containing perdeuterated leucine residues at one or two pre-selected positions, in mixed Langmuir monolayers with a phospholipid. The results presented here are more definitive than prior work employing x-ray reflectivity. They show explicitly that the di-helical peptide retains its designed α -helical secondary structure at the interface, when oriented perpendicular to the interface at high surface pressure, with the helices projecting into the aqueous subphase without penetrating the layer of phospholipid headgroups.

DOI: 10.1103/PhysRevE.70.061905

PACS number(s): 87.14.Ee, 68.18.-g, 87.64.Bx, 87.16.Dg

INTRODUCTION

One approach to develop “biomolecular” materials is to utilize artificial peptides designed with a simple, stable structural motif to exhibit a particular functionality, either biological or nonbiological, at the molecular level. Importantly, the motif must also be designed to facilitate their organization into ordered ensembles at the macroscopic level. Thus the designed molecular functionality can be translated into a macroscopic material property. For example, previously designed four-helix bundle motifs [1], with apposed histidine residues at selected positions within the bundle for the bis-histidyl coordination of metallo-porphyrin based prosthetic groups, can be used to generate interesting electron transfer [2–4] and nonlinear optical properties [5,6] at the molecular level. These can be vectorially oriented at a macroscopic interface also through their design [7]. However, one must necessarily ascertain whether the molecular structures as designed are indeed manifest at the interface in order to ensure that the intended molecular functionality can result in the desired material properties.

Specular neutron reflectivity, coupled with the deuteration of selected amino acid residues readily achieved via solid-phase chemical synthesis, can provide the desired structural information at near-atomic spatial resolution. Our purpose here is to demonstrate that capability with single monolayer samples (as opposed to thick multilayer samples [8,9]). Neutron scattering-length density (SLD) profiles can now be derived unambiguously from single monolayers of vectorially oriented peptides at liquid-vapor, liquid-liquid, solid-vapor, or solid-liquid interfaces. In the absence of a solid, recently developed, model-independent refinement methods may be used to derive these profiles with no *a priori* assumptions for monolayers at liquid-vapor or liquid-liquid interfaces [10]. When a solid is present, well-developed interferometric methods may be used [11]. We may apply these techniques

to neutron reflectivity data collected from two monolayers prepared identically except that one contains an unlabeled (all ^1H) peptide while the other contains a peptide labeled with a single perdeuterated (i.e., maximally $^1\text{H} \rightarrow ^2\text{H}$ substituted) residue at a pre-selected position in its amino acid sequence. The SLD profiles of the labeled monolayer will be the same as that of the unlabeled monolayer plus a contribution due to the extra SLD of the perdeuterated residue, which can be modeled as a simple Gaussian function. Nonlinear regression can then localize the perdeuterated residue with an accuracy of $\pm 0.5 \text{ \AA}$ within the profile structure of the monolayer of the vectorially oriented peptide. This approach can also be utilized with similar accuracy employing two perdeuterated residues at preselected positions in the peptide’s sequence, even if their separation is less than the spatial resolution of the derived profiles. The second approach can reduce the number of data sets required by a factor of approximately 2.

The results demonstrate explicitly that the alkylated di- α -helical peptide denoted BBC16 retains its α -helical secondary structure over most of its length, when the orientation of the helical axes is perpendicular to the interface at higher surface pressures in mixed Langmuir monolayers with the phospholipid dilauroyl phosphatidylethanolamine (DLPE), namely when the helical axes are aligned along the profile structure of the monolayer. This is accomplished by determining the positions, and hence the separations, of these selected residues within the monolayer profile structure to an accuracy of $\pm 0.5 \text{ \AA}$. Furthermore, the helices project into the subphase without penetrating the layer of phospholipid headgroups. The phospholipids thus compensate for the mismatch between the cross-sectional area of the α helix and that of the alkylating C16 hydrocarbon chain in the plane of the monolayer, as engineered by employing a phospholipid/peptide mole ratio of 2:1.

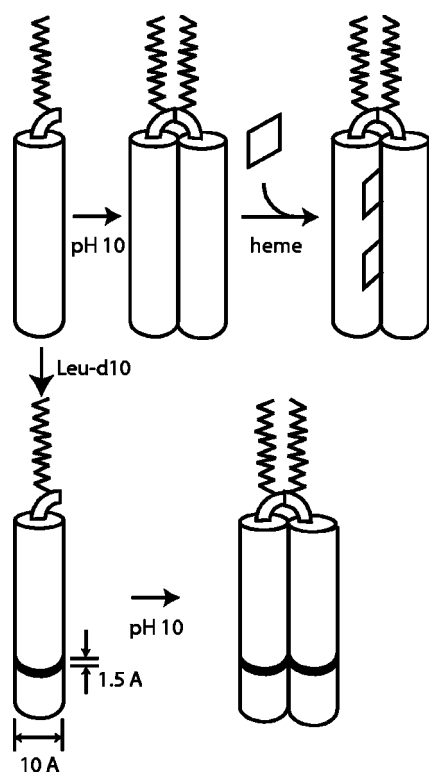


FIG. 1. Schematic representation of the di- α -helical peptide BBC16, synthesized as a mostly α -helical 31-mer with a flexible Gly₃ linker ending in an *N*-terminal Cys with a palmitoyl (C₁₆) chain attached and then dimerized in air under basic conditions to form BBC16. Heme dissolved in dimethyl sulfoxide added to the peptide can bind at *bis*-His ligation sites incorporated in the design. When the peptide is prepared with ²H-labeled Leu-d₁₀ at selected sites in the sequence, the contrast of the individual residue relative to the rest of the helix is enhanced. Dimensions indicate the average diameter and rise/residue of an α helix.

MATERIALS AND METHODS

Synthesis of ²H-labeled peptides

Peptides were synthesized by solid phase methods with *Fmoc* chemistry using a commercial machine (MilliGen), except that automated synthesis (which requires fourfold excess of each amino acid) was interrupted to permit manual coupling of a deuterated leucine residue at appropriate positions within the sequence of the peptide, with final coupling of the *N* terminus to perdeuterated palmitic acid also accomplished manually. The synthetic unit [CD₃(CD₂)₁₄-CGGGE IWKLH EEFLK KFEEL LKLHE ERLKK L-CONH₂] is homodimerized to form BBC16 (Fig. 1) [7,12]. In a series of singly labeled peptides, a Leucine residue at position 9, 14, 21, or 28 in the α -helix's sequence was replaced with Leucine with a perdeuterated (D₁₀) sidechain. In a series of doubly labeled peptides, either the Leucines at positions 9 and 21, or the Leucines at positions 14 and 28, were perdeuterated. Additionally, in the doubly labeled experiment, one histidine was mutated to alanine (H10 \rightarrow A) so that the resulting di-helices had only a single heme binding site. *Fmoc*-D₁₀-Leu (Leu-d₁₀) was purchased by custom order from CDN Isotopes (Pointe-Claire, Canada) and used without fur-

ther purification. Along with a fivefold excess of HOBT and diisocarbopropyl diimide, a 20% excess of Leu-d₁₀ was added to the resin in a DMF solution overnight. The resin was rinsed and unreacted peptide was capped with acetyl anhydride before the resin was returned to the column and automated synthesis resumed. Perdeuterated palmitic acid (PA_{D31}) (as received from CDN Isotopes) was used in the palmitoylation step for all the peptides used in this study. After dimerization, the peptide was lyophilized.

Langmuir monolayer preparation

Spreading solutions were prepared from the lyophilized peptide. Typical solutions were 100 μ M in 1 mM phosphate buffer with 10 mM NaCl, pH 8. In all cases the apo form (i.e., without a bound metalloporphyrin prosthetic group) of the peptide was used. DLPE (dilauroyl phosphatidylethanolamine) with perdeuterated (D₄₆) lauroyl chains (D-DLPE) was purchased by custom order from Avanti Polarlipids (Alabaster, AL) as a 1 mg/mL chloroform solution and used as received. Mixed monolayers in a 2:1 ratio of DLPE:BBC16 were spread as described previously [7], but with only a single stage deposition. The resulting isotherms were similar to those published [7].

Neutron reflectivity: Langmuir monolayers of singly and doubly labeled BBC16

Data from Langmuir monolayers of singly labeled and doubly labeled BBC16 in mixed monolayers of 2:1 D-DLPE:BBC16 were collected on separate experimental runs on the NG7 reflectometer at the Center for Neutron Research at the National Institute of Standards and Technology, Gaithersburg, MD. For the singly labeled monolayers, constant pressure control of the monolayers was not available, so monolayers were compressed to a surface pressure $\pi=40$ mN/m and the barrier then held fixed during the measurement. Data collection began about 30 min after compression, during which time π relaxed and stabilized to about 35 mN/m. We collected neutron reflectivity data as a function of the momentum transfer normal to the interface containing the monolayer, $Q_z=(4\pi/\lambda)\sin(\alpha)$, with α the incident angle and the wavelength $\lambda=4.768$ Å. The energy resolution of the instrument was $\Delta\lambda/\lambda=2.5\%$. Scans of the Q range investigated ($0.01 < Q_z < 0.2$ Å⁻¹) required about 4 h. Data from up to four consecutive scans were summed together. Except for one 4-h scan of the unlabeled D-DLPE/BBC16 monolayer on a D₂O buffer subphase, all data were collected on H₂O subphases (1 mM TRIS buffer, pH 8; unregulated room temperature, ≈ 22 °C).

For the doubly labeled monolayers, constant pressure mode was implemented during the run so that most of the data was collected at fixed $\pi=35$ mN/m. The monolayers were spread on either a pure D₂O subphase or a 50% D₂O/50% H₂O mixture. We used similar data collection times for scans over the range $0.01 < Q_z < 0.24$ Å⁻¹.

X-ray reflectivity: Langmuir monolayers of doubly labeled BBC16

Isomorphism of the Langmuir monolayers composed of doubly labeled D-DLPE/BBC16 was checked with x-ray re-

fectivity data collected on the Liquid Surface Spectrometer at CMC CAT, sector 9 of the Advanced Photon Source, Argonne National Lab. A different trough with constant- π feedback control (set for $\pi=35$ mN/m) and temperature regulation (22 °C) was used, but monolayer preparation was otherwise identical as for the doubly labeled neutron reflectivity measurement. Using incident photons of $\lambda = 1.23984$ Å, reflectivity scans over the range $0.010 < Q_z < 0.7$ Å⁻¹ required about 70 min.

Analysis of reflectivity from Langmuir monolayers

For the Langmuir monolayers containing the singly labeled BBC16 on an H₂O subphase, the scaling of the specular neutron reflectivity for the differently labeled peptides was complicated by the absence of total external reflection of the incident neutrons for $0 < Q_z < Q_c$. However, a simple scaling of the data sets to each other was achieved by noting that the inverse Fourier transform of the Fresnel-normalized reflectivity data in the first or second Born approximation is the autocorrelation of the gradient of the neutron scattering-length density (SLD) profile [10]. Consideration of this autocorrelation at $z=0$ Å readily demonstrates that the integral of the Fresnel-normalized reflectivity data is then equal to the integral of the square of the gradient SLD. On an H₂O subphase, the square of the gradient SLD is dominated by the features representing the hydrocarbon-air and hydrocarbon-peptide interfaces. This is true for all of the singly labeled and unlabeled BBC16 peptides because of the perdeuteration of the hydrocarbon chains of both BBC16 and the phospholipids DLPE. Thus the Fresnel-normalized reflectivity data for these monolayers were scaled to each other by simply setting their integrals equal to 1. However, we note that while this additional integral normalization procedure properly scales the resulting SLD profiles to each other placing them on the same arbitrary scale, it cannot provide for an absolute scale for the SLD profiles without further assumptions. In spite of this, the SLD profiles derived from these integral-normalized data, as described below, are sufficient for our purposes here, namely to localize the labeled residue within the monolayer SLD profile.

The above scaling approach could also have been applied to the Fresnel-normalized reflectivity data for the monolayers containing the doubly labeled BBC16 peptides but we avoided this issue by using D₂O and 50:50 D₂O/H₂O subphases with an experimentally accessible critical angle for total external reflection of the incident neutrons. As a result, the specular reflectivity data for the different monolayers, labeled and unlabeled, could be simply scaled to the Fresnel reflectivity near and below the critical angle via nonlinear least-squares fitting. This rigorous scaling procedure places the SLD profiles, also derived as described below, on the same absolute scale.

We have shown that the phase problem for specular x-ray and neutron reflectivity from thin films on liquid surfaces can be solved in the distorted-wave Born approximation [10]. The gradient of the scattering-length density (SLD) profile normal to the plane of the surface is bounded in these cases. This provides a powerful constraint allowing the phase prob-

lem to be solved with no *a priori* assumptions via an iterative Fourier refinement procedure applied to the Fresnel-normalized reflectivity. This approach has been termed “box refinement,” where “box” refers to the bounded nature of the gradient SLD profile. The critical boundary condition can be determined experimentally from the autocorrelation of the gradient profile obtained via an inverse Fourier transform of the Fresnel-normalized reflectivity without phase information. The phase solution and the resulting gradient SLD profile can be shown to be unique, and therefore unambiguously determined, when all of phase space is systematically explored for particular cases, especially for thin films on liquid surfaces. This gradient SLD profile can then be integrated either numerically, or better, analytically to provide the scattering-length density profile itself [10]. The analytic integration is achieved via the nonlinear least-squares fitting of the sum of a minimal number of Gaussian functions required to represent the resolved features in the gradient SLD profile. The SLD profile itself is then described by the corresponding sum of Error functions, their parameters fully determined from the fitted Gaussian functions.

This approach was utilized to derive the neutron SLD profiles for the fully hydrogenated peptides vectorially oriented in Langmuir monolayers at the air/water interface via sufficiently high surface pressure on subphases of pure D₂O, pure H₂O, and a 50:50 mixture. The neutron SLD profiles for the selectively deuterated peptides under otherwise identical experimental conditions were similarly derived. We note that isomorphism of the profile structures of the unlabeled and singly or doubly labeled Langmuir monolayers was demonstrated via specular x-ray reflectivity from such monolayers under otherwise identical experimental conditions (see below, Figs. 9 and 10). Such isomorphism is essential for the following.

The neutron SLD profiles for the case of the peptides containing a single perdeuterated residue on a H₂O subphase were then modeled as the sum of the neutron SLD profile for the fully hydrogenated peptide and a Gaussian function $(A/\sigma\sqrt{2\pi}) \exp[-(z-z_D^2/2\sigma^2)]$ representing the contribution of the perdeuterated residue, again via a nonlinear least-squares fitting of the Gaussian’s three parameters (amplitude A , width σ and position in the profile z_D). Note that this requires only that the neutron SLD profiles for the fully hydrogenated and selectively deuterated peptide cases be on the same arbitrary scale, as achieved with the integral normalization of the Fresnel-normalized reflectivity data described above for the case of the pure H₂O subphase. For the doubly labeled peptides on a subphase of either pure D₂O or a 50:50 mixture of D₂O/H₂O, the contribution of the two perdeuterated residues to the SLD profile of the fully hydrogenated peptide was modeled either as one or two Gaussian functions, requiring three or six independent parameters. Two Gaussians can represent each labeled site individually, while a single Gaussian would represent the average contribution from the pair of labels. Again, note that here, because of the total external reflection below Q_c , the neutron SLD profiles for the fully hydrogenated and selectively deuterated peptide cases are on the same absolute scale, as described above. All calculations involved in the derivation of the SLD profiles from the Fresnel-normalized specular x-ray or neutron re-

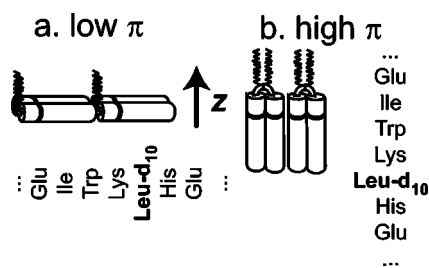


FIG. 2. At low surface pressure (a), the helices of BBC16 lie within the plane of the air/water interface and all residues are at the same position z relative to the interface. At high surface pressure (b), the helices orient with the helical axis approximately perpendicular to the interface and each residue is mapped onto a unique position z relative to the interface. Neutron reflectivity can then be used to determine the position of ^2H -labeled residues, such as Leu-d_{10} .

reflectivity data as described utilized code developed in MATHEMATICA. These calculations and the simulation of expected results neglected the finite energy resolution of the instrument. The nonlinear least-squares fitting of Gaussian functions as described employed the Levenberg-Marquardt algorithm, also as implemented in MATHEMATICA.

RESULTS

BBC16 monolayers were already characterized by chemical [12] and x-ray reflectivity methods [7,13], making them good systems for further structural investigation by neutron reflectivity. Key aspects of the peptide design and x-ray reflectivity results are summarized in Figs. 1 and 2. Off-specular x-ray scattering indicated that the in-plane structure of these Langmuir monolayers consists of a two-dimensional (2D) fluid of the vectorially oriented dihelices at the higher surface pressures [7]. Since there was no observable grazing incidence x-ray diffraction (GID) pattern, there was no direct information about the average tilt angle of the alpha helices. The electron density profile structures determined from x-ray reflectivity [7] (similar to those shown in Fig. 10: z values given below refer to this choice of origin) at the higher surface pressures could provide an estimate of the extent of the α -helical secondary structure of the peptide and/or the tilt angle of the helices with respect to the monolayer plane, based on a comparison of the monolayer thickness and the expected length of the α -helical peptide, but the complexity of the system makes this not so simple. The interactions between the phospholipid and the hydrocarbon chains of the peptide are difficult to predict because on average, the lipid and peptide hydrocarbon chains have excess area available compared to fully compressed alkyl chains, and the loop region of the peptide is flexible by design. Only part of the monolayer is composed of relatively rigid components, namely the helices. From the peptide design and the well-known properties of alpha helices, which have a rise of 1.5 Å/amino acid (Fig. 1), we expect that residues 5-31 should form a helix 40.5 Å long, with approximately constant electron density along its length. If we *assume* that the helical part of the peptide spans the region of uniform electron den-

sity between the monolayer/subphase interface centered on $z = -55$ Å and the interface with the phospholipids headgroups, centered at $z = -15$ Å in the monolayer electron density profile, then it is clear that the profile is consistent with α helices of the expected length with possibly only a very small tilt angle with respect to the normal to the monolayer plane. However, from the x-ray data there is no way of locating any particular residue, for example residue 5, the first residue of the helix nearest the N terminus which is alkylated, since its mean electron density is about the same as that of the other residues, as well as that of phospholipid headgroups, so we cannot be sure that the helices do not penetrate the headgroups. Computerized molecular modeling could lead to more sophisticated interpretations of the monolayer electron density profile, but we sought more definitive experimental data as could be provided by neutron reflectivity, coupled with the perdeuteration of selected leucine residues within the helices.

Neutron reflectivity from Langmuir monolayers of BBC16 with one selected perdeuterated residue

Neutron specular reflectivity measurements on Langmuir monolayers made with selectively deuterated BBC16 can provide a set of key distance measurements probing the intra-molecular structure of apo-BBC16—see Fig. 2. Simulations of the neutron reflectivity for apo-BBC16 on a H_2O subphase with perdeuterated palmitoyl chains and deuterated leucine residues at primary sequence positions 09, 14, 21, or 28 predicted good sensitivity to the sequence position of the deuterated amino acid, shown in Figs. 3(a) and 3(b). The initial neutron reflectivity from such Langmuir monolayers exhibited the expected sensitivity to the deuteration of a selected single leucine residue [14] shown in Figs. 3(c)–3(e). These data were first analyzed via a model-refinement of the deuterated residue position in the monolayer neutron SLD profile, which was based on the monolayer's electron density profile, against the neutron reflectivity difference data for the peptide containing the deuterated leucine residue vs the fully protonated peptide [14]. This model-dependent approach was modestly successful indicating that the localization of the deuterated residues in the monolayer profile structure could, in principle, be determined to an accuracy of about ± 1.5 Å. However, these model SLD profiles could only qualitatively predict the “sinusoidal” dependence of the neutron reflectivity difference data on the position of the perdeuterated residues, as opposed to quantitatively to within the experimental counting statistics. This model-dependent approach may have failed at the quantitative level because of a lack of isomorphism between the monolayers employed for the x-ray vs the neutron reflectivity experiments. Subsequently, we applied the model-independent box-refinement procedure employing only the known finite extent of the gradient of the monolayer neutron SLD profile. This approach provided the absolute neutron SLD profiles for both the deuterated leucine-containing peptide vs the fully protonated peptide at relatively low spatial resolution. Inspection of the difference between two profiles (e.g., Leu28 minus Leu14) showed a single maximum at the position of residue 28 and a single

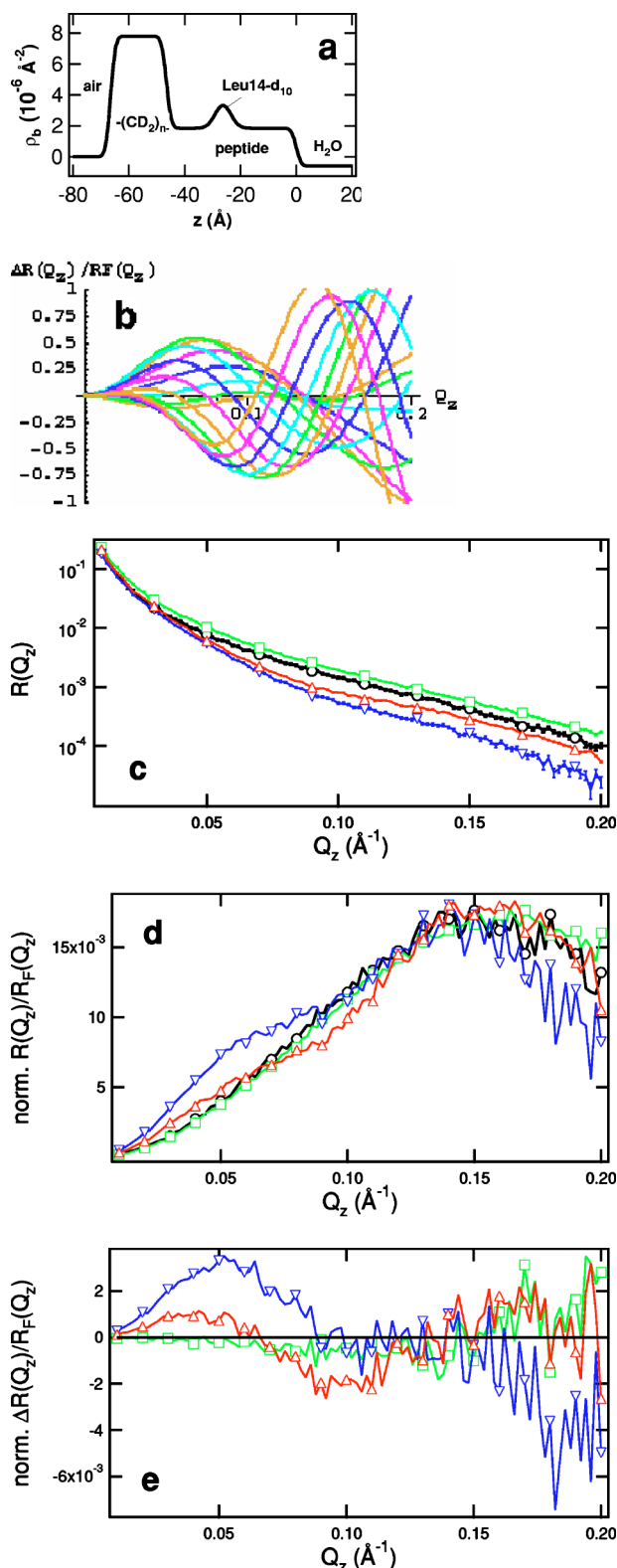


FIG. 3. (Color online) Model SLD profile structures for Langmuir monolayers of BBC16 based on the electron density profile structures obtained from x-ray reflectivity data. The H₂O subphase extends to the right for $z > 0$ Å; air extends from $z < -65$ Å (consistent with Fig. 4; other figures use a different convention). The perdeuterated hydrocarbon chains contribute to a region of high SLD ($-65 < z < -45$ Å) while the peptide has uniform, relatively low SLD, except at the label site, where Leucine is replaced by Leu-d₁₀ (here in the 14 position of the sequence). A series of model profile structures in which the label site was moved in 3 Å increments (every other sequence position) was used to generate a series of simulated Fresnel-normalized reflectivity curves, $R_{label}(Q_z)/R_F(Q_z)$ (not shown). The differences between these simulated reflectivities and the simulated reflectivity generated from the unlabeled model profile, $R_{nolabel}(Q_z)/R_F(Q_z)$, $\Delta R(Q_z)/R_F(Q_z) = R_{label}(Q_z)/R_F(Q_z) - R_{nolabel}(Q_z)/R_F(Q_z)$, (b), exhibit a sinusoidal variation over the experimentally accessible range of momentum transfer and its frequency is highly sensitive to the position of the deuterated residue within the monolayer profile structure. Such selectively deuterated minus fully hydrogenated difference data are routinely employed in structure analysis via neutron scattering, as they exploit the difference in the deuterium versus hydrogen atomic scattering factors for neutrons to the maximal extent (see Ref. [14]). (c) Experimental neutron reflectivity data $R(Q_z)$ collected from Langmuir monolayers spread from mixtures of the apo form of the synthetic peptide BBC16 and the phospholipids DLPE on a H₂O subphase at high surface pressure with the hydrocarbon chains perdeuterated and the peptide either undeuterated (black), with Leucine 09 deuterated (green), with Leucine 14 deuterated (blue), or with Leucine 28 deuterated (red). (d) The same data after both Fresnel and integral normalization, $norm. R(Q_z)/R_F(Q_z)$. The latter integral normalization of the Fresnel-normalized reflectivity data places the data on the same, but arbitrary scale (see Methods section). For clarity, error bars have been omitted, but this noise level, which increases with larger Q_z , is readily apparent from the point-to-point fluctuations in the data along Q_z as shown [see, for example, Fig. 5(b)]. (e) Difference data computed from the data in (d) between the experimental data for the peptide with a selected deuterated Leucine residue and that for the fully protonated peptide, $norm. \Delta R(Q_z)/R_F(Q_z)$, again on the same arbitrary scale. The sensitivity of these data to the sequence position of the selected deuterated Leucine residue is clearly evident. The “sinusoidal” variation in the difference data arises from the position of the single deuterated residue in the monolayer profile structure, as predicted by the simulated data shown in Fig. 3(b), irrespective of the different ordinate scales.

minimum at residue 14. Even this relatively crude method localized the label positions with an accuracy of about ± 1.5 Å.

More recently, the model-independent box-refinement procedure has been substantially improved [10,15]. The fully resolved features in the gradient SLD profiles, dp/dz derived via model-independent box refinement, are fitted with the

sum of a minimum number of Gaussian functions. The fitting is entirely objective and unambiguous since only the fully resolved features are modeled with arbitrary Gaussian functions employing the Levenberg-Marquardt algorithm for nonlinear regression analysis. The scattering-length density profile itself, $\rho(z)$, is then provided by direct analytic integration to provide a description of $\rho(z)$ in terms of a sum of

error functions whose parameters are entirely defined by those of the fitted Gaussian functions. Thus the SLD profile for the fully protonated peptide was so determined. The corresponding SLD profiles for the peptide with deuterated leucine at the 09, 14, and 28 sequence positions were then subjected to a more rigorous analysis. These profiles were fitted with the same SLD profile for the fully protonated peptide plus a single arbitrary Gaussian function feature representing the perdeuterated leucine residue in the SLD profile for the labeled peptides, with only the parameters of the Gaussian representing the labeled leucine as free parameters (i.e., amplitude, width, and position). These fits, again via nonlinear regression employing the Levenberg-Marquardt algorithm, provided the positions of the labeled residue within the monolayer profile structure to an accuracy of ± 0.5 Å, a threefold improvement (e.g., the asymptotic or estimated standard error for the 14 position was 0.344 Å and for the 28 position was 0.532 Å). There was no correlation (e.g., less than 0.0033 for the 14 position and less than 0.058 for the 28 position) with the other parameters and the residuals in real space were uniformly distributed at less than the 2% level, as shown in Fig. 4 for the perdeuterated leucine at the 14 position in the sequence.

The reader might ask at this point how a perdeuterated residue can be located within the monolayer profile to this high accuracy of ± 0.5 Å when the spatial resolution of the derived neutron SLD profiles is relatively low, namely only ≈ 30 Å. First, the Fresnel normalized neutron reflectivity data is sensitive to the position of the one perdeuterated residue over the corresponding range of Q_z , namely $Q_z < 0.25$ Å⁻¹, when the largest separation between its mean position in the monolayer profile and those of the other features which dominate the gradient SLD profile (the hydrocarbon/air and hydrocarbon/peptide interfaces with perdeuterated hydrocarbon chains) is comparable to this spatial resolution. This condition was met for the 14 and 28 sequence positions, but apparently not the 09 position. Second, given this relatively low spatial resolution of ≈ 30 Å, the Gaussian fit to the deuterium label distribution within the SLD profile must therefore necessarily be of comparable width. However, we know independently that the deuterium-labeled residue must in fact be located in a relatively narrow distribution in the monolayer profile because only one leucine residue has been labeled covalently, as made possible by the solid-phase chemical synthesis of the BBC16 peptide. Thus while this approach cannot determine this much narrower width, the mean position of the distribution in the monolayer profile can be accurately determined based on the first consideration above.

Neutron reflectivity from Langmuir monolayers of BBC16 with two selected perdeuterated residues

The improved model-independent box-refinement approach has now been applied to apo-BBC16 containing two perdeuterated leucine residues at sequence positions 09 and 21 and positions 14 and 28. The separations between the two residues for the first pair would be ≈ 18 Å and the second pair would be ≈ 21 Å in the monolayer profile for the

BBC16 di-helices oriented perpendicular to the monolayer plane at higher surface pressures. The neutron reflectivity data are shown in Fig. 5. The neutron SLD profile for the doubly labeled peptide at the 09 and 21 positions, as compared with that for the fully hydrogenated peptide, on pure D₂O subphase is shown in Fig. 6. The best fit of the neutron SLD profile for the fully hydrogenated peptide, plus a single Gaussian representing the average contribution of the two perdeuterated leucine residues, as compared to the SLD for the doubly labeled peptide, is also shown in Fig. 6, along with the residuals from the fit. The best-fit single Gaussian is centered at $z = -28.36 \pm 1.0$ Å in the monolayer profile. Utilization of two independent Gaussians representing the contribution of each labeled residue in the nonlinear fitting could not improve the fit, namely reduce the residuals below the level shown in Fig. 6. Similar results for the average position of these two perdeuterated residues in the monolayer profile were obtained independently, employing a different monolayer on a subphase of 50% D₂O and 50% H₂O, a substantially different neutron SLD contrast for the peptide portion of BBC16. The neutron SLD profile for the doubly labeled peptide at the 14 and 28 positions, as compared with that for the fully hydrogenated peptide, on a pure D₂O subphase is shown in Fig. 7. The best fit of the neutron SLD profile for the fully hydrogenated peptide, plus a single Gaussian representing the average contribution of the two perdeuterated leucine residues, as compared to the SLD for the doubly labeled peptide, is also shown in Fig. 7, along with the residuals from the fit. The best-fit single Gaussian is centered at $z = -32.87 \pm 0.65$ Å in the monolayer profile. However, the residuals for this best fit are significantly greater than those shown in Fig. 6 for the 09 and 21 pair of labeled residues, especially nearer the surface of the subphase. Utilization of two independent Gaussians could significantly improve the fit in this case, namely reduce the residuals below the level shown in Fig. 7, as shown in Fig. 8. The initial intent was that each Gaussian in the nonlinear fitting could represent the contribution from each labeled residue. However, this interpretation is unlikely given that one of the best-fit Gaussians had an area greater than three times the area of the other, together with the location of the minor Gaussian at the surface of the D₂O subphase. Instead, this minor Gaussian most likely represents the perdeuterated leucine residues within a small fraction of the di-helices lying on the subphase surface, their separate contributions being superimposed at this location in the monolayer profile structure for this orientation of the helices. The major Gaussian therefore is taken to represent the average contribution of the two perdeuterated leucine residues in the much larger fraction of di-helices oriented with their axes perpendicular to the subphase surface, their average position in the monolayer profile structure then being located at $z = -37.52 \pm 0.29$ Å. With this identification, the separation of the average position of the 09 and 21 labeled leucine residues, from that for the 14 and 28 labeled residues, is 9.16 Å in the monolayer profile structure. This compares well with the expected value of 9.0 Å [the difference in the average of the 09 and 21 positions, namely 15, and the average of the 14 and 28 positions, namely 21, is 6 residues at 1.5 Å per residue along the axis of an α helix (Fig. 1) provides an expected separation of 9.0 Å]. Further-

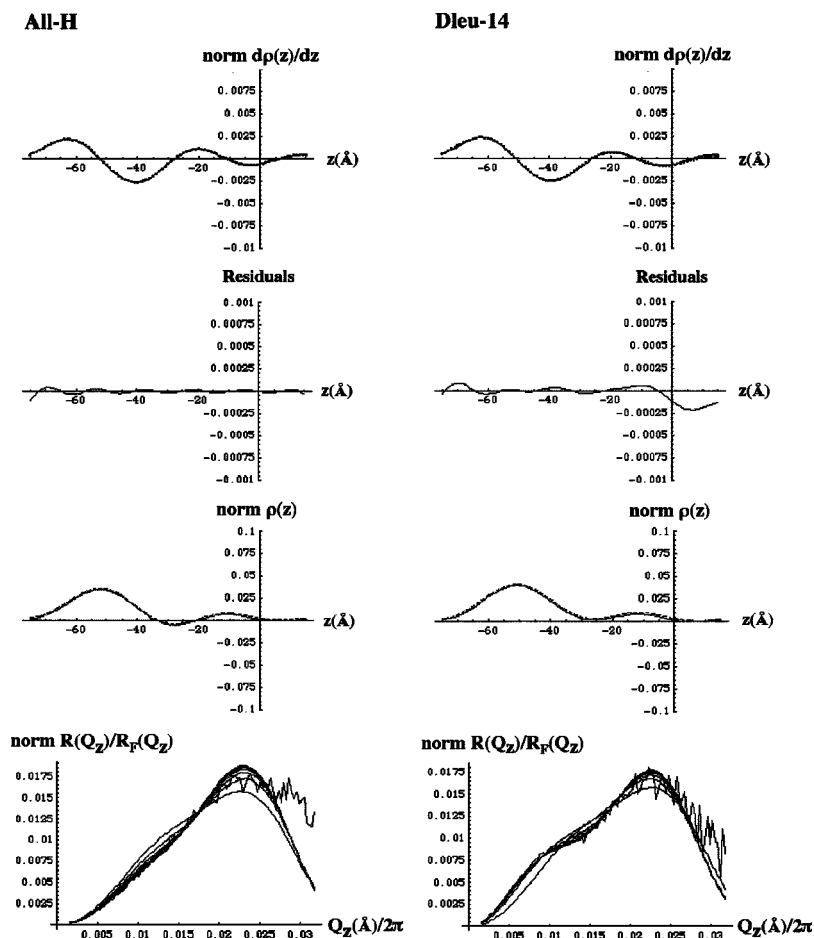


FIG. 4. Real-space analysis for fully protonated BBC16 peptide (all-H; left-column) and BBC16 peptide containing a perdeuterated leucine at sequence position 14 (Leu-d₁₀-14; right column). Top row left: Experimental gradient SLD profile, $\text{norm } d\rho(z)/dz$, from box refinement (dotted) vs the best model 4-Gaussian model from nonlinear fitting (solid) for the all-H case. Top row right: Experimental gradient SLD profile, $\text{norm } d\rho(z)/dz$, from box refinement (dotted) vs the same best 4-Gaussian model of the gradient SLD profile for the all-H case plus the additional best derivative of an arbitrary Gaussian representing the deuterium labeled residue from nonlinear fitting (solid). Second row: The corresponding residuals from the nonlinear fitting. Third row: numerical integral of the experimental gradient SLD profiles (dotted) vs the analytic integral of the corresponding best fitting model representations of the gradient SLD profiles, namely the SLD profiles themselves, $\text{norm } \rho(z)$, containing four error functions in the all-H case and the same four error functions plus a Gaussian function in the Leu-d₁₀-14 case. The perdeuterated hydrocarbon chains are localized within the $-60 < z < -40$ Å region in these SLD profiles. The small differences in the SLD profiles between the all-H and Leu-d₁₀-14 cases, readily apparent in the region occupied by the peptide, namely $-40 < z < 0$ Å, arise exclusively from the position of the perdeuterated leucine-14 residue in the SLD profile represented by a Gaussian function whose position is thereby determined by the nonlinear fitting to an accuracy of ± 0.5 Å [compare with the model profile structure on an absolute scale in Fig 3(a).] [Simple models, such as that shown in Fig. 3(a) were useful in planning the experiment, but required modification in several respects before they could be used to approximately account for the experimental neutron reflectivity. The water content of the monolayer decreased the contrast between the peptide and the subphase, the disorder of the perdeuterated hydrocarbon chains reduced their SLD, and the experimental resolution made features less prominent. Even with these modifications, the model-independent box-refinement method for obtaining the profile gradient, and its analytic integration providing the profile itself (third row of Fig. 4) did a much better job of explaining the observed data (as compared with Fig. 7(c), Ref. [14].)] Fourth row: The gradient of these SLD profiles in the top row clearly account for their corresponding Fresnel and integral normalized reflectivity data, $\text{norm } R(Q_z)/R_F(Q_z)$, to within the counting statistics for $Q_z/2\pi < 0.025$ Å⁻¹. The experimental data show the counting statistics in the point-to-point fluctuations in the data along Q_z as shown and the obvious effect of the perdeuterated leucine at sequence position -14, while the smooth curves simply demonstrate the convergence of the box refinement to the experimental data. Note that all of the ordinate scales in this figure are arbitrary, as they are linked to the integral normalization of the experimental Fresnel-normalized reflectivity as described in the text, and so indicated via the prefix “norm.” Nevertheless, these arbitrary scales for $\text{norm } R(Q_z)/R_F(Q_z)$, and therefore also $\text{norm } d\rho(z)/dz$ and $\text{norm } \rho(z)$, are the same for the fully hydrogenated vs the selectively deuterated cases allowing their direct comparison.

more, these average positions can be used to predict the actual positions of the perdeuterated leucine residues at the 09, 14, 21, and 28 positions within the monolayer profile structure, as well as the positions of the ends of the helices,

namely sequence positions 05 and 31. These positions are shown on the monolayer x-ray SLD (or electron density) profiles, as shown superimposed in Fig. 10 for all three monolayers demonstrating the isomorphism of the monolay-

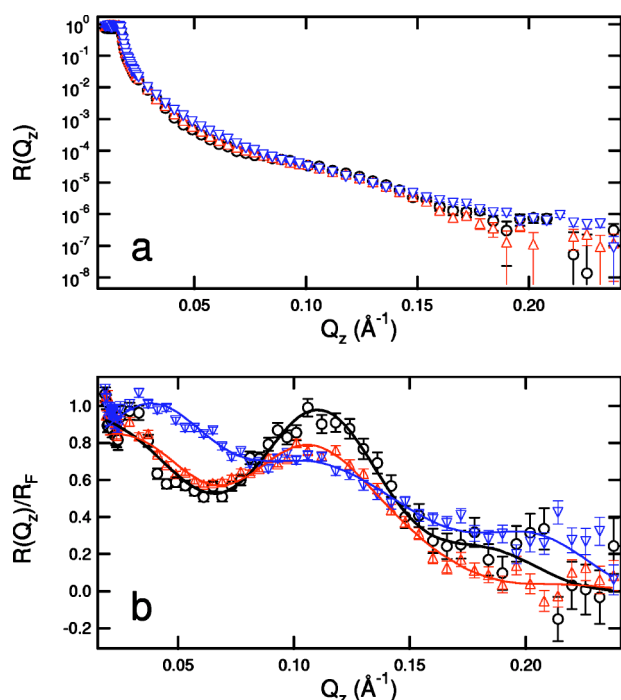


FIG. 5. (Color online) (a) Specular neutron reflectivity data collected from Langmuir monolayers composed of 2:1 D-DLPE:BBC16, in which the BBC16 had perdeuterated chains and was otherwise either unlabeled (\circ), or doubly labeled with D_{10} -Leucine either at positions 9 and 21 (red \triangle), or at positions 14 and 28 (blue ∇), all on a D_2O subphase (b). The same data after Fresnel-normalization (symbols) as well as the best fits obtained from box refinement (curves) (bottom). These data are on an absolute scale, as described in the text. Note that the point-to-point variations in the data, e.g., as for $R(Q_z)/R_F(Q_z)$ in Fig. 3(b), are the same magnitude as the error bars of the counting statistics, because the data were collected at intervals of Q_z much smaller than the widths of any of the maxima/minima in the data arising from features in the gradient SLD profile with maximal separation, the gradient SLD profile being of finite extent [8].

ers independent of the selected deuteration of the peptides (see Fig. 9). As can be seen, the so-predicted positions of the ends of the helices are in excellent agreement with the monolayer electron density profiles, considering that the electron-rich feature centered at $z = -10$ Å is due to the headgroup of the DLPE [7]. This indicates that the α -helical design of the peptide is not substantially modified by incorporation into the monolayer, and that the helices are indeed oriented with their helical axes normal to the interface. The alpha-helical portion of the peptide does not penetrate the headgroups of the phospholipids, but the loop part does. The proximity of the high-SLD lipid headgroups to Leu9 apparently masked the single Leu- d_{10} label and prevented us from extracting its position in the earlier single-label experiment. It is therefore noteworthy that the double-label experiment does not have the same problem. The agreement between the best-fit parameters and the expected change in SLD due to the presence of the labels is not as good, demonstrating that the experiment is more sensitive to the position of the labels than to their relative amplitudes. The data here can also be compared with the x-ray crystal structure [16] and the NMR solution

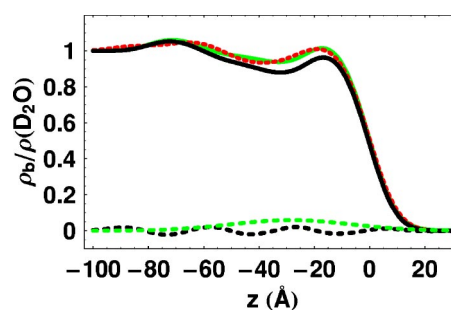


FIG. 6. (Color online) Comparison of SLD profile structures on an absolute scale from the doubly labeled peptide experiment. Solid black (dashed red): analytically integrated SLD profile from the unlabeled peptide (peptide labeled at Leu21, Leu09) with perdeuterated chains on a D_2O subphase. In both cases, the sum of five Gaussians was used to fit $d\rho/dz$. Solid green: the best fit to the labeled peptide SLD profile (dashed red) using the sum of the unlabeled SLD profile (black) plus a Gaussian with floating parameters. The best-fit Gaussian, shown in dashed green, is centered at $z = -28.36 \pm 1.0$ Å with a width of 21.63 ± 1.0 Å. The residuals appear as a black dashed curve. The ordinate is normalized by the SLD of D_2O ($6.25 \times 10^{-6} \text{ Å}^{-2}$). Thus the Gaussian has an integrated area corresponding to $20.0 \pm 0.8 \times 10^{-6} \text{ Å}^{-1}$. Assuming an area of $100 \text{ Å}^2/\alpha$ helix, the observed net change in total scattering length is $20 \pm 0.8 \times 10^{-12} \text{ cm}$, in good agreement with expectations for the double label (which exchanges $20 \text{ }^1\text{H}$ for ^2H ; $\Delta b_{total} = 20 \times 1.028 \times 10^{-12} \text{ cm} = 20.56 \times 10^{-12} \text{ cm}$).

structures [17]. For the crystal structure, the separation between the α carbons of the labeled residues is also nearly ideal, i.e., 1.5 Å/residue (e.g., L14-L21: 10.55 ± 0.01 Å; L21-L28: 10.45 ± 0.15 Å), while the NMR structures exhibit more

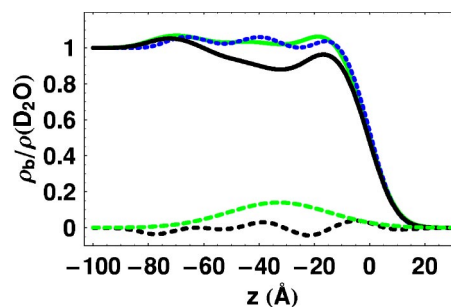


FIG. 7. (Color online) Comparison of SLD profile structures on an absolute scale from the doubly labeled peptide experiment. Solid black (dashed blue): analytically integrated SLD profile from the unlabeled peptide (peptide labeled at Leu28, Leu14) with perdeuterated chains on a D_2O subphase. For the unlabeled peptide (black), the sum of five Gaussians fit $d\rho/dz$, while for the labeled peptide (dashed blue), six Gaussians were necessary. Solid green: the best fit to the labeled peptide SLD profile (dashed blue) using the sum of the unlabeled SLD profile (black) plus a Gaussian with floating parameters. The best-fit Gaussian, shown in dashed green, is centered at $z = -32.87 \pm 0.65$ Å with a width of 18.37 ± 0.65 Å. The residuals appear as a black dashed curve. The ordinate is normalized by the SLD of D_2O ($6.25 \times 10^{-6} \text{ Å}^{-2}$). Thus the Gaussian has an integrated area corresponding to $40.4 \pm 1.2 \text{ Å}^{-1}$. Assuming an area of $100 \text{ Å}^2/\alpha$ helix, the observed net change in total scattering length is $40.4 \pm 1.2 \times 10^{-12} \text{ cm}$, about twice as large as expected for the double label.

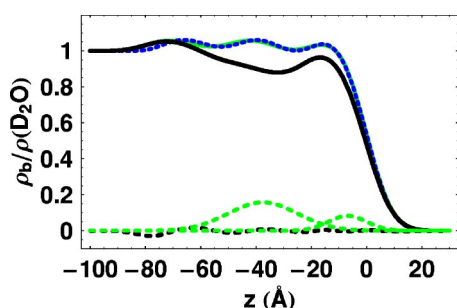


FIG. 8. (Color online) Comparison of the same SLD profiles on an absolute scale as in Fig. 7, unlabeled peptide (solid black) and Leu28,Leu14 doubly labeled peptide (dashed blue). Here, the solid green curve shows the best fit to the dashed blue curve by the sum of the unlabeled profile (solid black) plus two Gaussians, shown as dashed green curves. The Gaussian on the left is centered on $z = -37.52 \pm 0.29$ Å, with a width of 12.56 ± 0.32 Å and an integrated area of 31.1 ± 0.6 Å⁻¹, while the Gaussian on the right is centered at $z = -6.84 \pm 0.40$ Å, with a width of 6.90 ± 0.39 Å and an integrated area of 8.99 ± 0.53 Å⁻¹. Residuals are shown as a dashed black curve.

supercoiling, resulting in smaller separations (L14-L21: 10.0 ± 0.4 Å; L21-L28: 9.9 ± 0.1 Å). The monolayer data appear more consistent with the x-ray crystal data than with the solution structure.

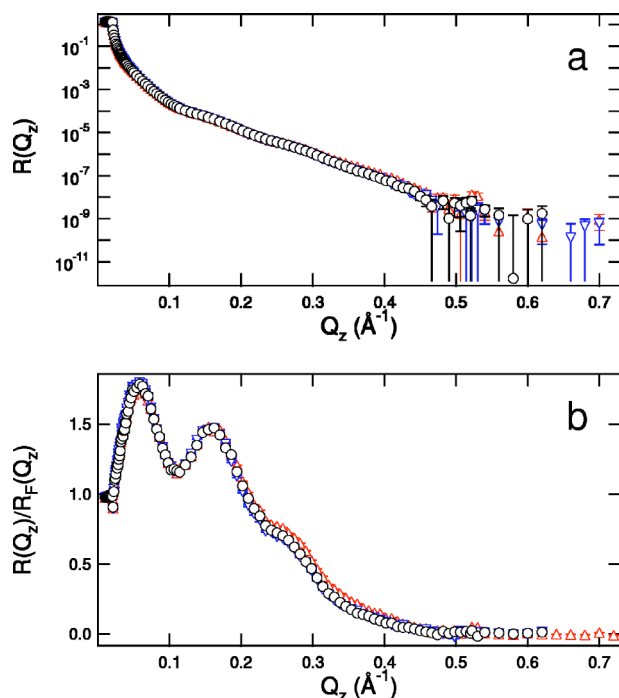


FIG. 9. (Color online) Specular x-ray reflectivity data collected from Langmuir monolayers composed of 2:1 D-DLPE:BBC16, in which the BBC16 had perdeuterated chains and was otherwise either unlabeled (○), or doubly labeled with D₁₀-Leucine either at positions 9 and 21 (red △), or at positions 14 and 28 (blue ▽), before (a) and after (b) Fresnel normalization, the latter on an absolute scale. The reproducibility of the results leads to the isomorphic electron density profile structures shown in Fig. 10.

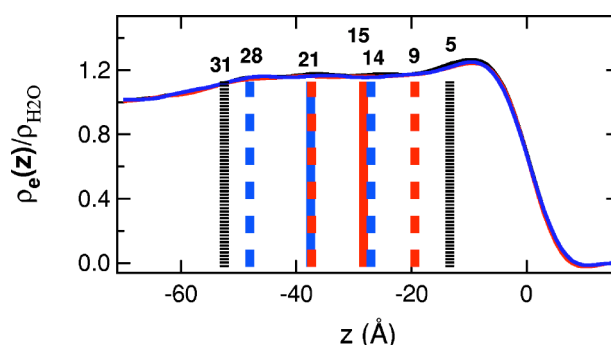


FIG. 10. (Color online) Electron density profile structures on an absolute scale for 2:1 D-DLPE:BBC16 obtained by numerically integrating the profile gradients derived by box refinement from the x-ray reflectivity data shown in Fig. 9(b). Black: unlabeled; red: doubly labeled at Leu21,09; blue: doubly labeled at Leu28,14. The solid vertical lines show the centers of the excess SLD due to the double labels as determined from the neutron results in Figs. 6 and 8, that is, they should correspond to the positions of residues 21 and 15, as indicated. The dashed vertical lines show the corresponding positions of the individual labels that can be deduced by assuming the peptide is perfectly α helical, while the dotted vertical lines indicate where residues 5 and 31, the ends of the helical portion of the peptide, would be based on the same reasoning. (The electron dense feature to the right of position 5 is due to the headgroups of D-DLPE.)

CONCLUSION

We have demonstrated that it is now possible to determine the positions of single perdeuterated residues within the profile structure of single monolayers of vectorially oriented artificial peptides with an accuracy of ± 0.5 Å, employing specular neutron reflectivity and a model-independent method of analysis, so-called box-refinement. It is essential that the fully hydrogenated and selectively deuterated peptide monolayers be isomorphous, as can be demonstrated by specular x-ray reflectivity. For artificial peptides based on α -helical bundle structural motifs which can be vectorially oriented perpendicular to the plane of the monolayer, the structural information provided by such determinations for a selected set of perdeuterated residues within an artificial peptide, each determination undertaken separately, can be utilized to ascertain whether the peptide's structure as designed has been maintained or modified by its incorporation into the monolayer ensemble. In this case, we find that the peptide maintains its α -helical secondary structure. These α helices are untilted and oriented normal to the interface at high surface pressure. They do not penetrate the phospholipid headgroups. Now that we have demonstrated the technique's sensitivity and developed the necessary analytical tools, we can apply it to ask whether the incorporation of prosthetic groups modifies the structure of the peptide in the monolayer. If so, classical molecular-dynamics simulations of the monolayer system may be used to indicate the nature of the structural modification, using the experimentally determined positions of the labeled residues within the monolayer profile structure as key constraints. Development of next-generation neutron sources should greatly facilitate these measurements, so that

the precision with which the profile structure can be dissected will only be limited by the effort needed to prepare differently labeled monolayers.

ACKNOWLEDGMENTS

The authors thank Robert Ivkov, Andrey Tronin, and Songyan Zheng for help with the singly labeled experiments at NIST; Larry Kneller for help with the doubly labeled experiments at NIST; Nicholas Maliszewskij and Mathieu Doucet for help with the trough software at NIST; Elaine DiMasi, Thomas Gog, Chitra Vankataraman, and Diego Casa

for assistance at CMC CAT; Shixin Ye for help with the comparison to crystal and NMR structures; Charles Majkrzak for helpful comments on this manuscript. This work was supported by the NIH (Grant No. GM55876) and the MRSEC program of the NSF under Award No. DMR96-32598. We acknowledge the support of the National Institute of Standards and Technology, U.S. Department of Commerce, in providing the neutron research facilities used in this work, as well as additional support from the Cold Neutrons in Biology and Technology Partnership/NIH RR14812. Use of the Advanced Photon Source was supported by the U.S. Department of Energy, Office of Science, Office of Basic Energy Sciences, under Contract No. W-31-109-ENG-38.

-
- [1] D. E. Robertson, R. S. Farid, C. C. Moser, J. L. Urbauer, S. E. Mulholland, R. Pidikiti, J. D. Lear, A. J. Wand, W. F. DeGrado, and P. L. Dutton, *Nature (London)* **368**, 425 (1994).
- [2] K. Wynne, S. M. LeCours, C. Galli, M. J. Therien, and R. M. Hochstrasser, *J. Am. Chem. Soc.* **117**, 3749 (1995).
- [3] A. G. Hyslop and M. J. Therien, *Inorg. Chim. Acta* **276**, 427 (1998).
- [4] N. P. Redmore, I. V. Rubtsov, and M. J. Therien, *J. Am. Chem. Soc.* **125**, 8769 (2003).
- [5] S. M. LeCours, H. W. Guan, S. G. DiMagno, C. H. Wang, and M. J. Therien, *J. Am. Chem. Soc.* **118**, 1497 (1996).
- [6] V. F. Vance and J. T. Hupp, *J. Am. Chem. Soc.* **121**, 4057 (1999).
- [7] J. Strzalka, X. Chen, C. C. Moser, P. L. Dutton, B. M. Ocko, and J. K. Blasie, *Langmuir* **16**, 10 404 (2000).
- [8] G. Zaccai, G. Buldt, A. Seelig, and J. Seelig, *J. Mol. Biol.* **134**, 693 (1979).
- [9] G. Buldt, H. U. Gally, J. Seelig, and G. Zaccai, *J. Mol. Biol.* **134**, 673 (1979).
- [10] J. K. Blasie, S. Zheng, and J. Strzalka, *Phys. Rev. B* **67**, 224201 (2003).
- [11] L. R. Kneller, A. M. Edwards, C. E. Nordgren, J. K. Blasie, N. F. Berk, S. Krueger, and C. F. Majkrzak, *Biophys. J.* **80**, 2248 (2001).
- [12] X. Chen, C. M. Moser, D. L. Pilloud, and P. L. Dutton, *J. Phys. Chem. B* **102**, 6425 (1998).
- [13] J. Strzalka, X. Chen, C. C. Moser, P. L. Dutton, J. C. Bean, and J. K. Blasie, *Langmuir* **17**, 1193 (2001).
- [14] J. K. Blasie and P. Timmins, *MRS Bull.* **24**, 40 (1999).
- [15] S. Zheng, J. Strzalka, D. H. Jones, S. J. Opella, and J. K. Blasie, *Biophys. J.* **84**, 2392 (2003).
- [16] S. S. Huang, B. R. Gibney, S. E. Stayrook, P. L. Dutton, and M. Lewis, *J. Mol. Biol.* **326**, 1219 (2003).
- [17] J. J. Skalicky, B. R. Gibney, F. Rabanal, R. J. B. Urbauer, P. L. Dutton, and A. J. Wand, *J. Am. Chem. Soc.* **121**, 4941 (1999).